Morphologically templated nucleation of primary Si on AlP in hypereutectic Al-Si alloys

Xiangzhen Zhu[a], Shihao Wang[a], Xixi Dong[a], Xiangfa Liu[b*], Shouxun Ji[a*]

[a] Brunel Centre for Advanced Solidification Technology (BCAST), Brunel University London, Uxbridge, Middlesex UB8 3PH, United Kingdom

[b] Key Laboratory for Liquid-Solid Structural Evolution & Processing of Materials, Ministry of Education, Shandong University, Jinan 250061, China

* Corresponding author:

Xiangfa Liu, Tel.: +56 53188392006, Email: xfliu@sdu.edu.cn

Shouxun Ji, Tel.: +44 1895 266663, Fax: +44 1895 269758, Email: shouxun.ji@brunel.ac.uk

Abstract

AlP has been widely used as an effective heterogenous nucleus for primary Si phase in hypereutectic Al-Si alloys, but the morphological correlation between AlP and primary Si is still confusing. In the present work, the morphologies of AlP crystals were studied comprehensively by experimental observation and theorical prediction. It is found that AlP collected from an Al-0.03P melt could be divided into two categories: spinel twin crystals and non-twin crystals. During the nucleation process, these two kinds of AlP crystals triggered morphologically templated nucleation of primary Si phase, resulting in the formation of hexagonal primary Si twin and octahedral non-twin crystals, respectively. As such, the percentage of primary Si twin crystals in the experimental Al-18Si alloy was also increased obviously after the morphologically templated nucleation via AlP. The morphologically templated nucleation also eliminated the dendritic growth of primary Si phase and the formation of hopper structures inside primary Si, forcing primary Si to maintain to be faceted solid crystals through layer-by-layer growing mechanism. The insight into morphologically templated nucleation offers a new view in understanding the mechanism of heterogeneous nucleation of primary Si phase on AlP nuclei.

Key words:

Aluminium alloys; Solidification; Nucleation; Primary Si, Grain refinement; Morphology

1. Introduction

Al-Si alloys are predominately important casting alloys and have been extensively applied in different sectors of industry, which contributes 90% of all shaped castings [1]. In hypereutectic Al-Si alloys, it is generally believed that the size and morphology of primary Si phase are critical in determining the final mechanical properties, in particular the ultimate tensile strength and elongation of manufactured components. Therefore, the refinement of primary Si phase has been a popular topic for hypereutectic Al-Si alloys since phosphorous was reported to be able to refine primary Si phase [1]. At present, phosphorous-containing master alloys have been widely adopted in industry as a common and essential practice to achieve effective grain refinement in casting hypereutectic Al-Si alloys.

A lot of efforts have been made to elucidate the scientific fundamental mechanism of heterogenous nucleation of primary Si phase on AlP. It has been revealed that AlP has the same lattice structure (fcc) and very similar lattice parameters with Si phase (a_{AlP}=0.545nm, a_{Si}=0.542nm). Such a high structural similarity makes the nucleation of Si on AlP don't need the assist of intermediate phase or layer, which was reported to be necessary for other refining particles (such as TiB_2 [2, 3] and NbB_2 [4-7]) in Al melt. Therefore, AlP is a very effective heterogeneous nucleation substrates for primary Si phase [8]. The morphologies of primary Si phase and AlP were also extensively studied, revealing that two typical morphologies of primary Si phase in hypereutectic Al-Si alloys are octahedron without twin and hexagonal plate-like spinel twin which are all bounded by facetted {111} faces [9-13]. As for the morphology and growth mechanism of AlP, the reported evidence indicate that AlP crystals exist in the form of spinel twin [8-12]. In 1969, Hajimu [14]successfully grew a AlP single crystal from Al melt and found that AlP had a 2D shape of plate with exposed (111) face. In 1998, Lescuyer [15] observed plate-like and blocky AlP crystals and found that plate-like AlP embryos evolved into blocky crystals in Al melt when the holding time was increased. Zuo and Zhang [16, 17] also confirmed the existence of 2D morphologies of plate-like and

blocky AlP embryos, separately. Recently in 2010, the 3D morphology of AlP was successfully observed in the fracture surface of a Al-Si-P alloy and the results confirmed that AlP are typical spinel twin crystals [18]. From the view of geometry, spinel twin crystals can show plate-like and blocky morphologies in 2D, depending on (1) the aspect ratio of thickness and length, and (2) the position of section [11].

Generally, the re-entrant grooves existing in a spinel twin offers preferential positions for solute atoms to attach and thus the characteristics of a spinel twin can be retained in the newly formed outer layer of crystals [19]. From this point, it is easily understood that the primary Si particles nucleated on AlP spinel twin should be also twin crystals. However, the octahedral primary Si phase without twin was also often observed in hypereutectic Al-Si alloys [11, 12]. It is confusing why these octahedral primary Si phase do not inherit the twin morphological feature if they were also nucleated on AlP spinel twin nuclei. The possible reasons for the confusion can be speculated to (1) there is an unrevealed mechanism responsible for the transformation from twin crystals to non-twin crystals during the heterogeneous nucleation of primary Si phase on AlP twin nuclei, (2) AlP embryos exist in unrevealed non-twin forms which are responsible for the nucleation of octahedral primary Si phase. Besides, although both spinel twin and octahedron are widely considered as two basic morphologies of primary Si phase in hypereutectic Al-Si alloys, it is still unclear what's the percentage of each morphology and whether the phosphorous refinement has a significant effect on their percentages.

To further understand the heterogeneous nucleation of primary Si phase on AlP, a thorough investigation and understanding is required. However, the observation of AlP nuclei in hypereutectic Al-Si alloys is very difficult because (1) the ultralow concentration of AlP in alloy (200-600 ppm) makes it hard to locate and observe AlP crystals; and (2) the severe hydrolysis of AlP during specimen preparation often destroys their morphology, composition and structural features [14, 20]. Therefore, a new method/technique is necessary to overcome these difficulties. Recently, a pressurised melt filtration technique was successfully used to concentrate AlN

inclusions in aluminium melt [21]. During the filtering process, molten metal was forced by argon gas to flow through a micro filter disc, and the solid inclusions in the melt quickly built up and were enriched on the filter disc surface, creating an inclusion band for further metallographic analysis. AlP nuclei in Al-Si melt would precipitate as solid particles before the solidification of Al-Si melt. Therefore, the pressurised melt filtration technique also offers the opportunity to concentrate enough AlP crystals from Al melt with ultralow concentration of AlP to study the nucleation mechanism in hypereutectic Al-Si alloys.

In the present work, we aim to study the 3D morphologies of AlP crystals through experimental observation and theorical prediction. AlP crystals were collected from locally concentrated Al-0.03P melt. The sample were finally ion milled in a vacuum chamber to remove the reacted layer on AlP surface for further observation of twin structure and orientation relationship between AlP and Si, which can provide evidence for the morphological templated nucleation of primary Si phase on AlP. Discussion focused on the formation of 3D morphologies of AlP and the morphologically templated nucleation of primary Si phase on AlP nuclei.

2. Experimental process

The Al-18wt.%Si and Al-25wt.%Si base alloys (all compositions quoted in this paper are in wt.% unless otherwise stated) were re-melted at 850 ºC in a graphite crucible using an electric resistance furnace. The refinement treatment was carried out by adding premade commercial Al-3P master alloy. The designed concentrations of phosphorous (P) in the melt were 0, 200 and 400 ppm, and the tested phosphorous concentrations by optical emission spectrometer (OES, Foundry-master Pro) were 5, 186 and 370ppm, respectively. After adding the Al-3P master alloy and holding the melt at 850 ºC for 30min, the melt was manually stirred and subsequently poured into a permanent mould to make a casting with a size of 70 mm × 35 mm × 20 mm. After that, the samples were obtained from the centre of the casting, followed by a standard procedure of mechanical grinding and polishing. A further milling was applied in the vacuum chamber of a Gatan

precision ion polishing system (PIPS) at an incident angle of 4-6° and a voltage of 4 kV for 6 h to remove the reacted layer on AlP surface due to the severe hydrolysis during specimen preparation. To observe the 3D morphologies of primary Si phase, a 15 vol.% HCl-distilled water solution was used to completely remove the matrix of the samples, and then primary Si particles were collected utilizing a centrifugal extractor by segregating the solution.

To concentrate AlP crystals, a pressurised melt filtration technique was adopted. The Al-0.03P melt was prepared and holding at 850°C for 30 min, then poured into a pre-heated filtration crucible at 200°C in the sealed chamber of the pressure filtration equipment (Prefil®-Footprinter, ABB). Then argon gas was introduced into the chamber to force the melt through the porous ceramic filter fixed at the bottom of the filtration crucible. When the melt passed through the filter disc, precipitated AlP crystals were collected and concentrated immediately above the filter disc together with the remaining melt. As the remaining Al melt solidified, the concentrated samples were sectioned, grinded and polished. The details of the pressure melt filtration equipment and principles can be found elsewhere [22] [23]. The samples were further milled in the vacuum chamber of PIPS. The 3D morphologies of AlP crystals were studied by observing the fracture surface of a concentrated specimen, which was frozen with liquid nitrogen firstly to obtain the fracture section easily.

The microstructure characterization and crystal structure identification of the samples were carried out using optical microscope (OM) and field emission scanning electron microscopy (SEM) equipped with energy-dispersive x-ray spectroscopy (EDS) and electron back-scattered diffraction (EBSD).

3. Experimental Results

3.1 Effect of phosphorous refinement on the morphologies of primary Si phase

Figure 1 shows the as-cast microstructures of Al-18Si alloys before and after

phosphorous refinement via Al-3P master alloy. Clearly, the addition of Al-3P refiner resulted in a significant increase in the number density and a significant decrease of the average size of primary Si phase, which was 160 μm in the alloy without phosphorous, but was 83 μm and 28μm in the alloy with 200ppm and 400ppm phosphorous, respectively. This confirmed that phosphorous had an excellent refinement effect on primary Si phase, which is in good agreement with other results [24, 25]. The 2D morphologies of primary Si phase were presented as triangular, square, trapezoidal, and hexagonal outlines. No obvious difference in the 2D morphologies of primary Si phase was found before and after refinement. Meanwhile, there is also no existing literature paying attention to any morphological difference induced by phosphorous refinement. However, 2D images are unable to reveal the real geometry and thus it is still unclear whether the 3D morphologies are different. To clarify this issue, the 3D morphologies of primary Si phase need to be presented, which can be achieved through extraction techniques using 15 vol.% HCl-distilled water solution.

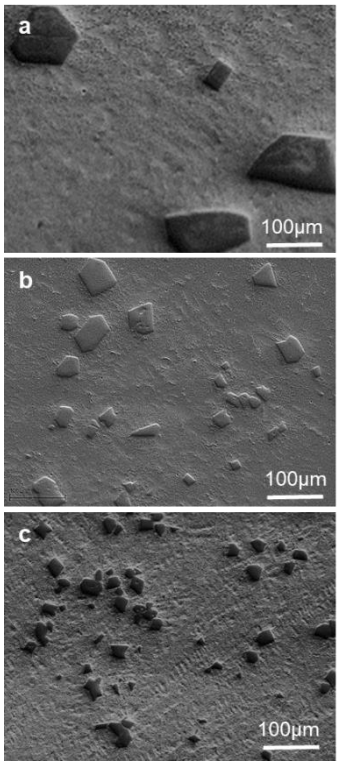

Figure 1. SEM images showing the microstructures of as-cast Al-18Si alloys: (a) unrefined, (b) refined by 200ppm P and (c) refined by 400ppm P.

Figure 2 shows the 3D morphologies of primary Si crystals extracted from an Al-18Si alloy. Among these morphologies, the most common one was the octahedron bounded by 8 faceted {111} faces. The other typical morphology was the spinel twin (Figure 2b), which could be obtained by rotating the lower half part of the octahedron crystal at 180° relative to the upper half part about the direction normal to (111). Therefore, such a spinel twin is also be bounded by {111} faces, and the twin plane was (111). The morphological feature of the spinel twin was that its side faces could be distinguished by three 141° twin grooves alternating with three 219° twin ridges. The standard spinel twin crystal showed triangular {111} upper and bottom faces, as shown in Figure 2b. While, according to the twin plane re-entrant edge (TPRE) growth theory [18, 26, 27], the twin grooves promoted the rapid growth of the side faces along <211> directions, resulting in the thin spinel twin plate with hexangular upper and bottom faces, as shown in Figure 2c. Therefore, the hexangular plate-like crystal is the majority of spinel twin crystals in the experimental alloys. Except the single twin crystals, a few hexangular plate-like primary Si crystals with multiple parallel or unparallel twins were also observed, as shown in Figure 2d-f.

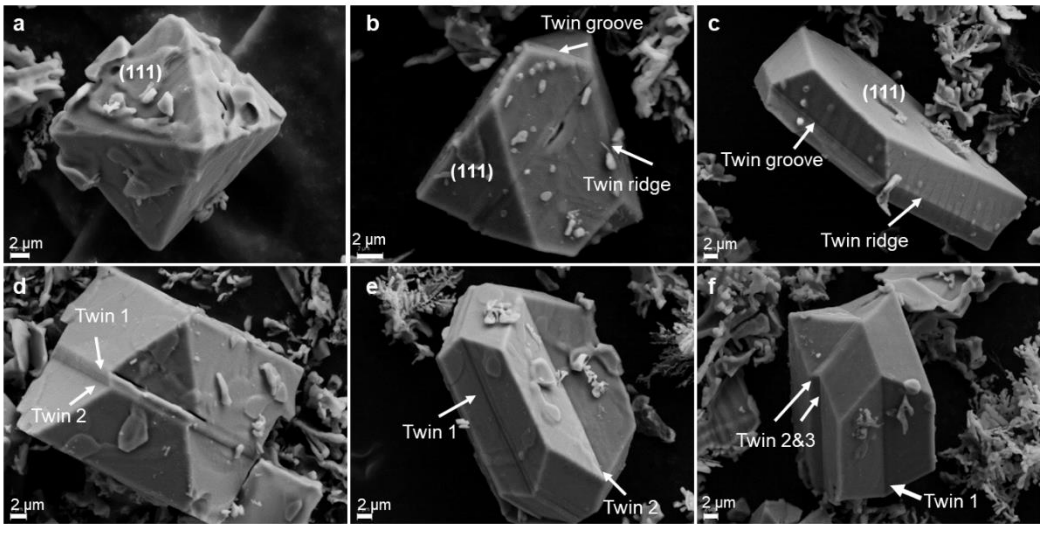

Figure 2. SEM images showing the 3D morphologies of primary Si phase in the Al-18Si alloy refined by Al-3P master alloy:(a) octahedron, (b) standard spinel twin, (c) hexangular plate-like spinel twin, (d) hexangular plate with parallel twins and (e, f) hexangular plate with unparallel twins.

From Figure 2, it is known that the primary Si crystals can be divided into 2 basic categories: (1) non-twin crystals (i.e., octahedral crystal without twin in Figure 2a) and (2) twin crystals (Figure 2b-f), although Si twin crystals have a series of morphological variations. To investigate the morphological difference induced by phosphorous refinement, EBSD technique was adopted to identify the percentage of twin crystals. Figure 3 shows the microstructure of the Al-18Si alloy without refinement and its corresponding combined inverse pole figure +image quality map (IPF+IQ), in which the two parts of a twin crystal were presented in 2 different colours. In this cross section, 66 primary Si crystals were observed and 12 of them were identified as twin crystals (marked by solid white circle). The enlarged figures and detailed EBSD investigation of more than 130 primary Si crystals in each experimental Al-18Si alloys (132 for Al-18Si-0P alloy, 198 for Al-18Si-0.02P alloy and 191 for Al-18Si-0.04P alloy) are shown in the Figure S1-S11 in the supplementary materials. According to the EBSD results, the percentage of primary Si twin crystals in 3 experimental Al-18Si alloys was summarized in Table 1. It was only 16.7% in the unrefined alloy but largely increased to 30.3% and 31.9% in the alloys refined by 200 ppm and 400 ppm phosphorous, respectively. This means that the primary Si non-twin crystals are always dominant in hypereutectic Al-Si alloys, but phosphorous refinement can promote the formation of Si twin crystals.

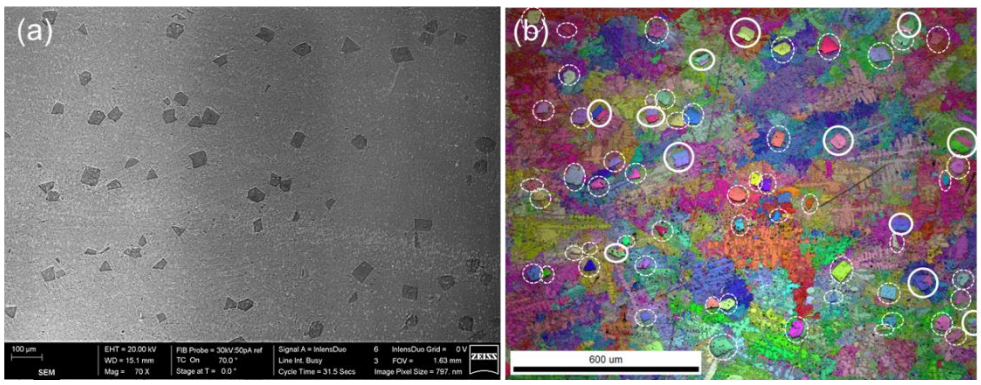

Figure 3. (a) SEM image of the unrefined Al-18Si alloy and (b) its corresponding combined inverse pole figure +image quality map (IPF+IQ), in which 66 primary Si crystals were observed. Among them, 12 twin primary Si crystals (marked by solid white circle) were

identified. The nontwin primary Si were marked by dashed white circle.

Table 1. The percentage of identified twin primary Si crystals in experimental Al-18Si alloys

Alloy	Al-18Si-0P	Al-18Si-0.02P	Al-18Si-0.04P
Number of identified twin crystals	22	60	61
Total number of observed crystals	132	198	191
Percent (%) of twin crystals	16.7%	30.3%	31.9%

3.2 Orientation relationship between primary Si and AlP nuclei

The experimental results in Figures 1-3 indicate that the existence of AlP, which was reported to be a twin crystal [18], promotes the formation of primary Si twin crystals. However, it was also found that the octahedral primary Si non-twin crystals were always the dominant crystals even after phosphorous refinement. This phenomenon causes confusion and raises the following questions: (1) do the octahedral primary Si non-twin crystals have AlP twin crystals as their heterogeneous nuclei? (2) if they have AlP twin nuclei, why does the twin morphological feature disappear in the primary Si after heterogeneous nucleation? To answer these questions and further elucidate the heterogeneous nucleation of primary Si on AlP, EBSD analysis was conducted to detect the orientation relationship between primary Si and AlP.

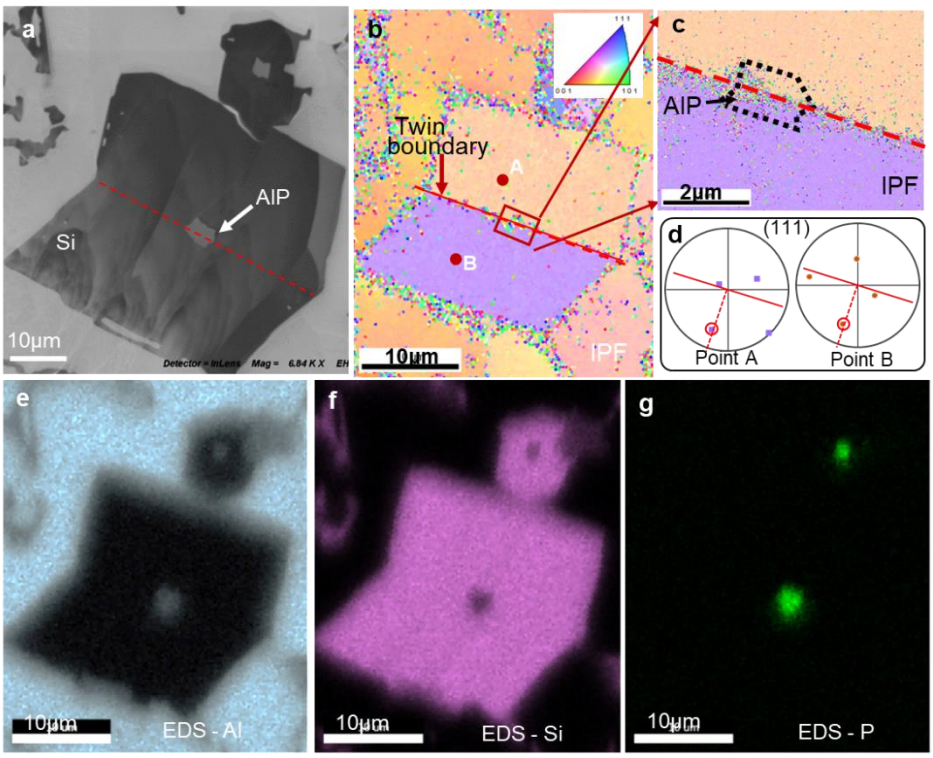

Figure 4. (a) Primary Si twin crystals and their AlP nuclei in the Al-18Si alloy refined by 200ppm P and its corresponding (b,c) IPF, (d) (111) pole figure of point A and B in (b), (e-g) EDS map of the primary Si shown in (a). Among them, (c) is the enlarged IPF with higher resolution corresponding to the area marked by red square in (b).

Figure 4a shows two primary Si particles in the Al-18Si alloy refined by 200 ppm P. In the central area of each primary Si particle, it is seen the existence of a grey phase, which was enriched in Al and P according to the EDS results (Figure 4e-g). Therefore, it was confirmed as AlP nucleus. The IPF map shown in Figure 4b preliminarily indicates that this primary Si particle is a twin crystal, and the twin boundary lines (marked by red dot line) crossed the AlP nucleus. Figure 4d shows the (111) pole figures of point A and B marked in Figure 4b. When a twin exists, the parent grain and its twin share one plane which is referred as the twinning plane. When illustrated on a pole figure, the position of the shared plane is normal to the orientation of the twin trace [28]. Figure 4d clearly illustrates the shared plane (the corresponding dot in pole figure are marked by red circle) is (111), further confirming that this primary Si is a twin crystal with a (111) twin plane. The enlarged IPF map with higher resolution (Figure

4c) provided more details for the nucleus area marked by red square in Figure 4b. It is found that the AlP nucleus has the same orientation with twin Si, thus is also a twin crystal and its twin boundary line coincided with that of primary Si twin crystal. Moreover, the IPF could not distinguish the phase boundary between AlP and Si, indicating that they had a typical cubic-to-cubic orientation relationship. From this evidence, it can be concluded that the primary Si crystal and the twin structure were epitaxially formed directly from a AlP twin crystal in a cubic-to-cubic orientation relationship.

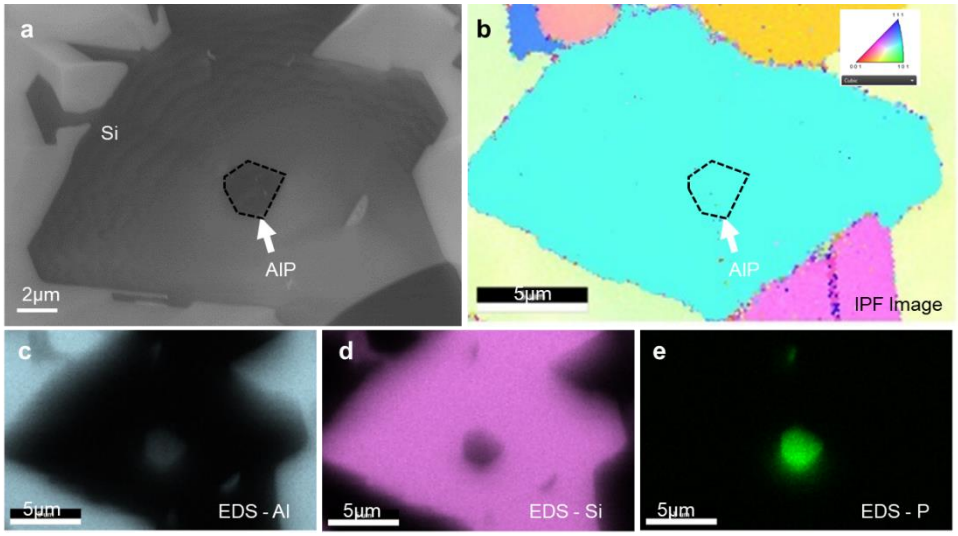

Figure 5. (a) Primary Si non-twin crystals and its AlP nucleus, and its corresponding (b) IPF and (c-e) EDS map.

Figure 5a shows another type of primary Si particle. The EDS results shown in Figure 5c-e indicate that this primary Si also had an AlP nucleus in its centre. The IPF map in Figure 5b revealed that both primary Si and its AlP nucleus were not twin crystals, but Si and AlP still exhibited a cubic-to-cubic orientation relationship. Based on the observed 3D morphologies of primary Si shown in Figure 2, it can be concluded that the primary Si non-twin crystal shown in Figure 5 should be an octahedral primary Si. Also, the AlP nucleus of this octahedral primary Si non-twin crystal was not a twin crystal. So, there should exist some unreported AlP non-twin crystals, which are responsible for the heterogenous nucleation of non-twin primary Si phase.

3.3 Revealing the 3D morphology of AlP in Al melt with ultralow concentration of phosphorous

To confirm the existence of the AlP non-twin crystals and reveal its 3D morphologies, AlP crystals were concentrated from an Al melt with ultralow concentration of 300ppm phosphorous by a pressurised melt filtration technique. Here it should be mentioned that the filtration equipment is just to enrich and collect the precipitated solid particles (i.e., AlP) but can't enrich the dissolved atoms in Al melt which could pass through the filter disc. Therefore, the solute atoms (i.e., P) concentration in melt, which is widely considered as a factor to control the 3D morphology of crystals, would not change due to filtration. In other word, the filtration technique applied in the present work would not change the morphology of AlP. On the other side, Si atoms in Al-Si-P melt were reported to have no significant effect on the dissolution of P atoms [15] and not to react with Al-P atomic clusters [29] or affect the precipitation and existence of AlP crystals [30]. Therefore, it can be speculated that AlP crystals in Al-P and Al-Si-P melt should be the same. However, it is not convenient to observe AlP in solidified Al-Si-P alloys because it would be wrapped by Si crystals. So, in the present work, we only observed AlP crystals in Al-P alloys.

Figure 6a shows the microstructure of the concentrated sample, in which a lot of grey or dark polygonal AlP crystals were observed in the matrix. Two typical AlP crystals are shown in Figure 6b and c, respectively. Although these two AlP crystals have similar hexagonal outlines in 2D sections, the corresponding IPF (Figure 6c and d) and (111) pole figures (Figure 6e) revealed that the one shown in Figure 6b was a twin crystal, but the one shown in Figure 6c was a non-twin crystal. This result preliminarily confirmed the existence of AlP non-twin crystals.

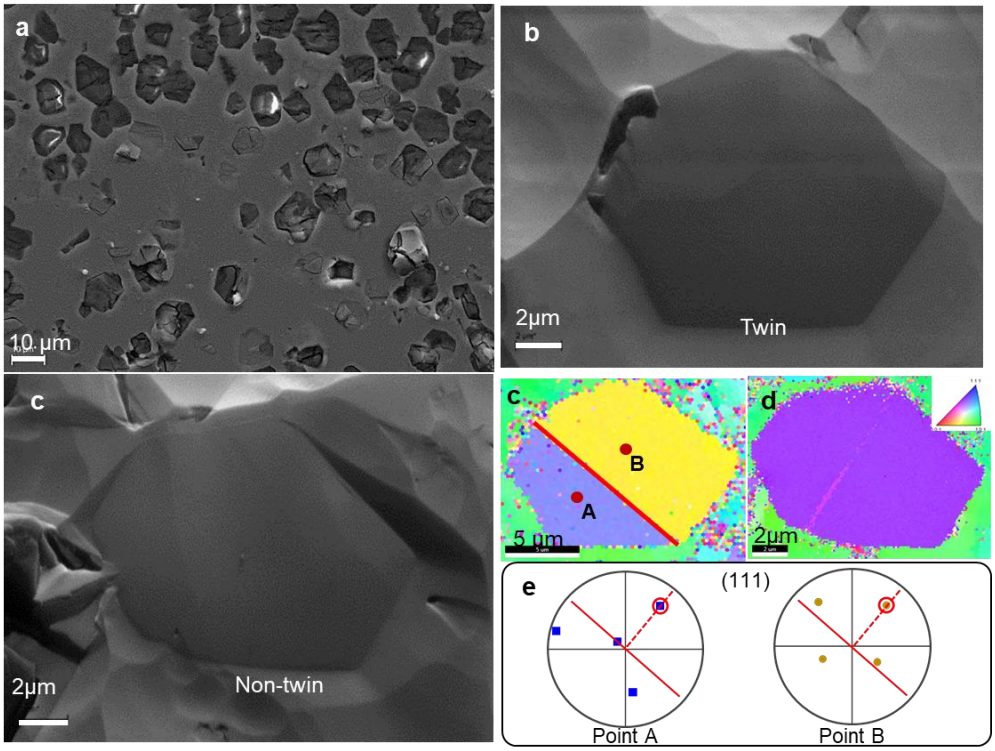

Figure 6. (a) Microstructure of the concentrated Al-0.03P alloy, (b, c) SEM images and (d,e) corresponding IPF maps of two typical AlP crystals, (f) (111) pole figure of point A and B in (c).

Figure 7 shows the 3D morphologies of AlP observed from the fractured surface of concentrated sample. Similar with the primary Si, AlP also has a common morphology of hexagonal platelet (i.e. spinel twin) as shown in Figure 7a. However, no variation of spinel twin was discovered yet. The AlP non-twin crystals were indeed observed and presented as four morphologies: octahedron, truncated octahedron, cuboctahedron, and cuboid, as shown in Figure 7b-e, respectively. Among them, truncated octahedron was dominated. This is clearly different with the morphology of primary Si crystals. Except the symmetric morphologies shown in Figure 7, some asymmetric morphologies of AlP were also observed. Figure 8 a and b show two typical asymmetric AlP crystals deviated from hexagonal plate-like twin and truncated octahedral non-twin crystals, respectively. Be different with the symmetric crystals, each asymmetric crystal had a unregular pentagonal face (marked by A and B, respectively).

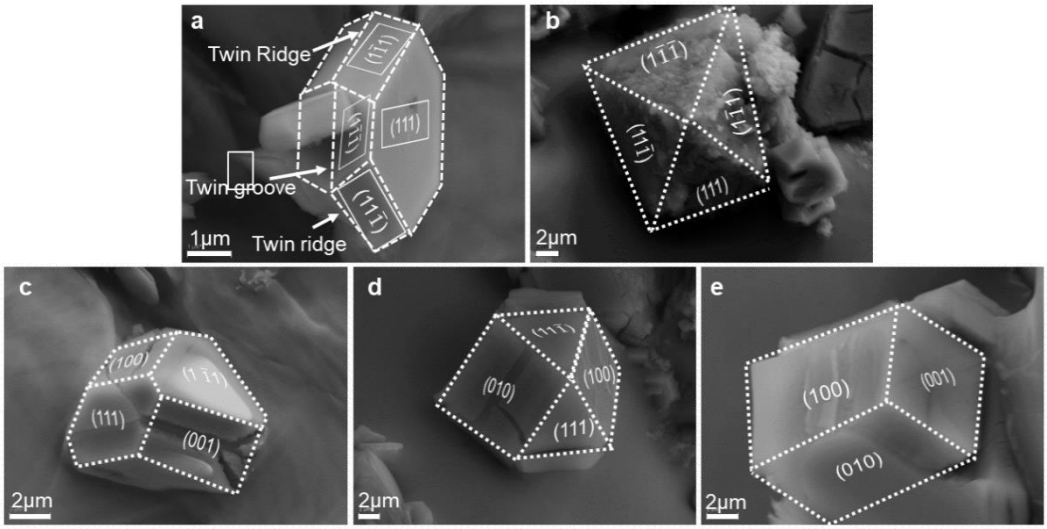

Figure 7. Typical morphologies of AlP crystals, (a) hexagonal platelets with a twin, (b) octahedron, (c) truncated octahedron, (d) cuboctahedron and (e) cuboid.

In summary, AlP crystals can also be divided into two categories: twin crystals and non-twin crystals. Be different with primary Si, AlP twin crystals only exist in the form of hexagonal plate-like spinel twin; while AlP non-twin crystals have a common morphology of truncated octahedron and three rare morphologies of cuboctahedron, octahedron, and cuboid. As a comparison, primary Si twin crystals have a series of morphological variations, but primary Si non-twin crystals only exist in the morphology of octahedron. However, the percentage of AlP twin crystals can't be calculated directly by a statistic analysis of 3D morphological observation or EBSD information, due to (1) A lot of AlP crystals are aggregated and sheltered by the Al matrix or other AlP crystals, and also cracked/deformed due to the stress induced by fracture of the concentrated sample, therefore their twin feature can't be identified accurately; (2) the reacted AlP parts also often found in the ion-polished sample and lost their initial crystal structure information, hindering the calculation the percentages of AlP twin crystals by a statistic analysis of EBSD information of a large number of AlP crystals.

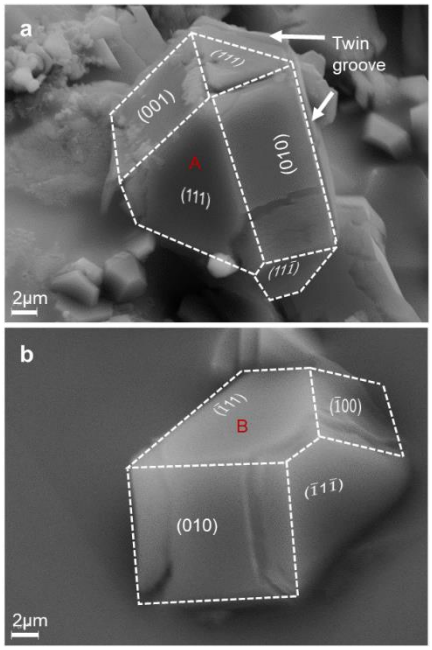

Figure 8. Asymmetric AlP crystals, (a) with and (b) without a twin. These are deviated from hexagonal plate-like twin and truncated octahedral crystals, respectively.

4. Discussion

4.1 The formation of 3D morphology of AlP

During the crystal growth process, the slower growing faces tend to retain last, thus have more probability of appearing in the final morphology as compared to the faster growing ones. The Bravais-Friedel-Donnay-Harker (BFDH) law [31, 32] is a well-accepted theory to predict crystal morphology from the view of the crystal lattice. According to the BFDH law, the equilibrium growth rate of a given {hkl} face is inversely proportional to the interplanar distance d_{hkl} after considering the extinction conditions of the crystal symmetry. AlP has a zincblende structure (space group F-43m, 216). Table 2 shows the morphological importance (MI) rank of AlP crystal faces according to the BFDH law. The MI rank of a (hkl) face is an index indicating the probability of that a face appearing in the morphology. The higher the MI rank, the larger the probability. In table 2, 1 and 6 are the highest and lowest MI rank, respectively. Table 2 also lists the corresponding simple forms, which are a set of crystal faces with the same atomic arrangement and related symmetry. The number of

faces contained in a form is called the multiplicity. The real crystal morphology can be considered as a combination of one or several simple forms.

Table 2. Morphologically important (MI) rank of AlP crystal faces calculated using the BFDH law and corresponding simple forms

MI rank	Face (hkl)	d (nm)	Multiplicity	Simple form
1	{111}	0.3154	4	Tetrahedron
2	$\{11\bar{1}\}$	0.3154	4	Tetrahedron
3	{200}	0.2732	6	Cuboid
4	{220}	0.1931	12	Rhombic dodecahedron
5	{311}	0.1647	12	Trigonal dodecahedron
6	$\{31\bar{1}\}$	0.1647	12	Trigonal dodecahedron

From Table 2, it is known that the top 2 important faces are {111} and $\{11\bar{1}\}$. Here it should be noticed that, although {111} and $\{11\bar{1}\}$ generate octahedron in many point groups, they may form 2 different but equally important simple forms in the point group -43m: positive and negative tetrahedrons [33]. When the positive and negative tetrahedrons are appeared together, the combinate form is octahedron, which was observed and shown in Figure 7. Meanwhile, {200} is the third important face and forms a simple form of cuboid, which was also observed in Figure 7e. Although the equilibrium morphology of AlP should be tetrahedron or octahedron, the variations in crystal growth conditions such as solution flow, concentration and impurities can lead to the modified growth kinetics of crystals and the appearance of faces with lower ranking of MI. When {111}, $\{11\bar{1}\}$ and {200} faces appeared at the same time, a series of combinate forms, including truncated octahedron, cuboctahedron and truncated cube, will be generated depending on the growth rate along <111> and <100> directions.

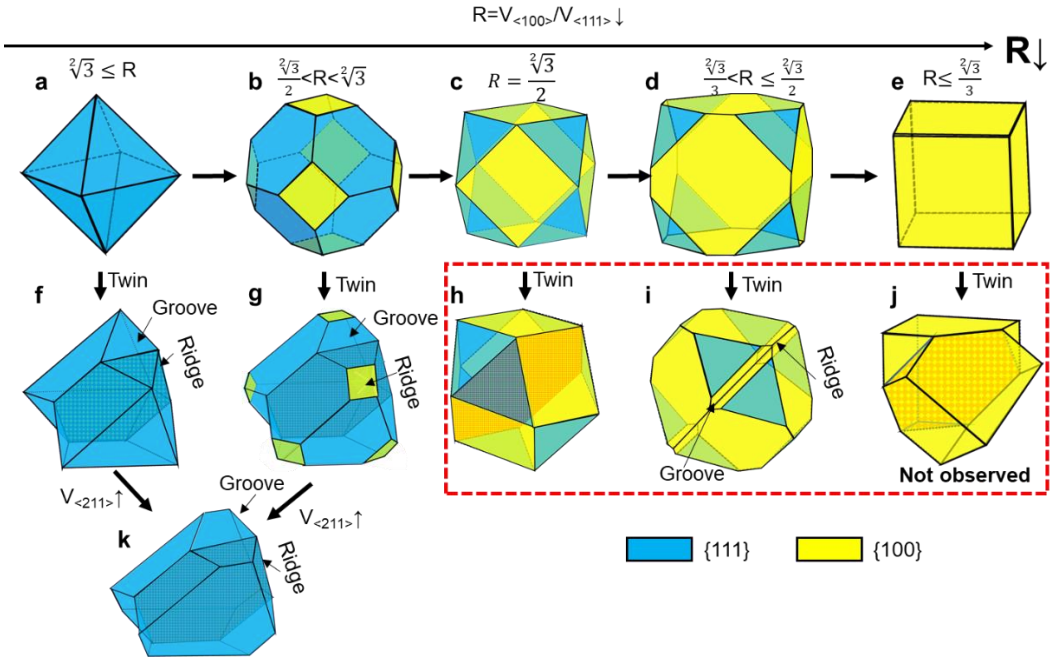

Figure 9. Sketch diagrams showing the typical AlP morphologies and their evolutional relationship.

Figure 9 shows the morphological evolution of AlP depending on the ratio R of the growth rates along the <100> ($V_{<100>}$) and <111> directions ($V_{<111>}$). As the single forms of positive and negative tetrahedrons always are appeared together and form a combinate of octahedron in the experimental alloy, it is not necessary to distinguish {111} and $\{11\bar{1}\}$. So, {111} can be used to represent both four {111} and four $\{11\bar{1}\}$ faces. If $R\geq\sqrt{3}$, the crystals will grow as an octahedron bounded only by eight {111} faces (Figure 9a). As R decreases from $\sqrt{3}$, six {100} faces appear and become more and more important, resulting in the formation of truncated octahedron with eight triangular {111} faces and six square {100} faces, as shown in Figure 9b. When R decreases to $\sqrt{3}/2$, a cuboctahedron with 8 hexagonal {111} faces and six square {100} faces can be obtained. As R further decreases, {100} faces become dominant for the exposed faces but {111} faces gradually disappear. During this process, AlP morphologies are evolved from truncated cuboid ($\frac{\sqrt{3}}{2}>R>\frac{\sqrt{3}}{3}$) to cuboid ($R\leq\frac{\sqrt{3}}{3}$), as shown in Figure 9 d and e.

Twin crystals can be formed by faulted stacking during crystal growth. It was reported that Si only needs one faulted atomic layer to form a twin and possesses a relatively small stacking fault energy of about 50-60 mJ/m^2, therefore it is easy to form Si twin with the (111) twin plane [34, 35]. Figure 9f and g show the twin crystals corresponding to octahedron and truncated octahedron, respectively. According to TPRE mechanism, the presence of 141° re-entrant grooves promotes the preferential deposition of Si atoms in the melt along <211> directions of solidifying Si crystals [18, 26, 27]. Such a growth is considered to be planar and isotropic. Consequently, it gives rise to the formation of hexagonal plate-like twin crystals, as shown in Figure 9k. Theoretically, the twin crystals corresponding to cuboctahedron, truncated cuboid and cuboid could exist, but have not been observed in the present work. While, to systematically elucidate the possible morphologies of AlP, these were also shown in Figure 9h-j.

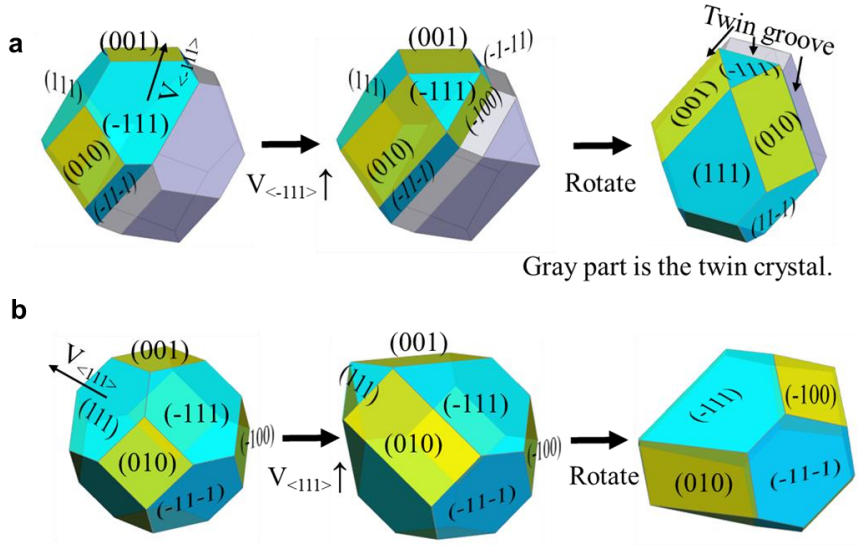

Figure 10. Sketch diagrams showing the formation of asymmetric AlP crystals deviating from truncated octahedron morphology and its twin as the result of increased growth rate along a certain [111] direction.

Crystal growth rate depends on the environmental conditions such as solution flow, concentration and impurities, which are always not uniform and/or can be severe

segregation or ever renewed interface in the melt. Therefore, it gives rise to the formation of asymmetric AlP crystals. Figure 10 shows the formation mechanism of two asymmetric AlP crystals that are shown in Figure 8 from the experimental observation. As the truncated octahedral crystal (Figure10b) or its corresponding twin crystal (Figure 10a) have an accelerated growth rate along a certain direction such as $<\bar{1}11>$ or <111> due to the inconsistent environmental conditions, the corresponding faces could extrude into melt quickly, resulting in the changes of faces in the adjacent area and outlines. For example, the accelerated $(\bar{1}11)$ hexagonal face could shrink into a small triangular face, and its adjacent hexagonal (111) face would evolve into an irregular pentagonal face, as shown in Figure 10a. After a rotation, this asymmetric AlP crystal could be observed in the position shown in Figure 8a.

4.2 Morphologically templated nucleation of primary Si phase on AlP nuclei

It has seen that the individual primary Si non-twin crystal has its AlP non-twin nucleus and the individual primary Si twin crystal also has its AlP twin nucleus inside. Moreover, there exists a cubic-to-cubic orientation relationship between primary Si and AlP nucleus. It means that AlP is the morphological template for primary Si during heterogeneous nucleation. Figure 11 shows the detailed process of the morphologically templated nucleation of primary Si on AlP crystals.

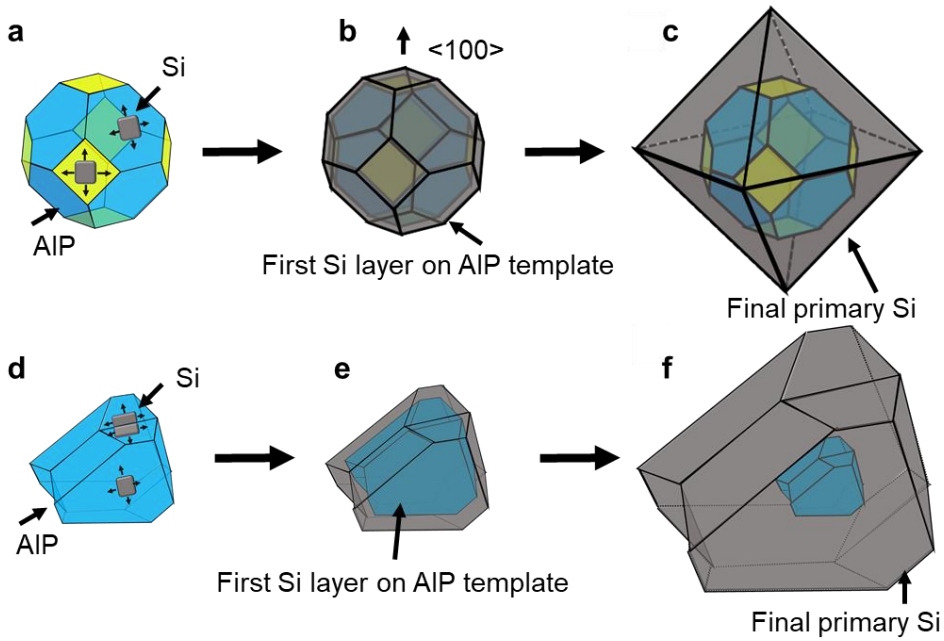

Figure 11. Sketch diagrams showing the morphologically templated nucleation of primary Si on AlP nucleus: (a,d) deposition and extension of two dimensional Si agglomerates, (b, e) the formation of first layer of faceted Si on AlP template, (c, f) final geometry of primary Si crystal after duplicating layer-by-layer growth.

As the decrease of melt temperature, faceted AlP template is firstly precipitated from the melt due to the ultralow solubility of P atoms in Al melt [15, 30, 36]. Taiji [37] reported that the calculated nucleation rate of primary Si in Al-16Si melt with an undercooling of 65K is almost 0, therefore concluded that the precipitation of primary Si is a heterogenous nucleation process and depends on the heterogenous nuclei. Due to the high structural similarity between Si and AlP, the precipitated AlP crystals offers a perfect heterogenous nuclei site for primary Si. According to the classic nucleation theory, Si atomic clusters moved randomly from melt to the exposed AlP faces and some of Si clusters are segregated and sedimented on the AlP crystal face in a cubic-to-cubic orientation relationship to form 2D Si crystal-like agglomerates, as shown in Figure 11 a and d. The edge of a Si agglomerates is not smooth at atomic level and offer rough step or kink sites at which the required bonding energy to incorporate new Si clusters is much less [38]. Therefore, 2D Si agglomerates can spread rapidly along the preferential direction by incorporating Si clusters from melt until the first Si layer

covers the whole AlP template, as shown in Figure 11 b and e. Due to the new Si layer maintains a cubic-to-cubic orientation relationship with AlP template, the twin structure in AlP twin crystals is also passed to the new Si layer. After the formation of first Si layer, new layer of 2D Si agglomerates can be crystalized and subsequently form the second layer of Si on top of the first layer. By duplicating this process, the layer-by-layer growth of primary Si continues till forming the whole grain or interrupted by solidification process. The concentric growth traces of primary Si (shown in Figure 12), which is the result of temperature fluctuation and impurity layer deposition, are the notable feature of morphologically templated nucleation and subsequent layer-by-layer growth mechanism [39, 40].

After the formation of first Si layer that covered the whole truncated octahedral AlP template, the subsequent growth would follow the growth habits of Si which are decided by both the internal crystal natures and external environmental conditions. On one hand, although Si and AlP have the same fcc lattice structure and very similar lattice parameters, Si crystal only contains Si atoms and covalent bond while AlP has two different atoms which are bonded by uncomplete covalent bond. On the other hand, the concentration of solute atoms, which is normally considered as a key factor affecting crystal morphology [40], are also in a big difference: P in melt is only several hundred ppm while Si can reach up to 18%. The abundant supply of Si atoms is helpful the preferential growth along the <100> ($V_{<100>}$), resulting in the disappear of exposed {100} faces, as shown in Figure 11c. Therefore, the final morphologies of AlP and Si are different, as shown in Figure 2 and 7. Similarly, primary Si twin crystals also have several morphological variations as shown in Figure 2, despite that AlP twin crystal only has one morphology.

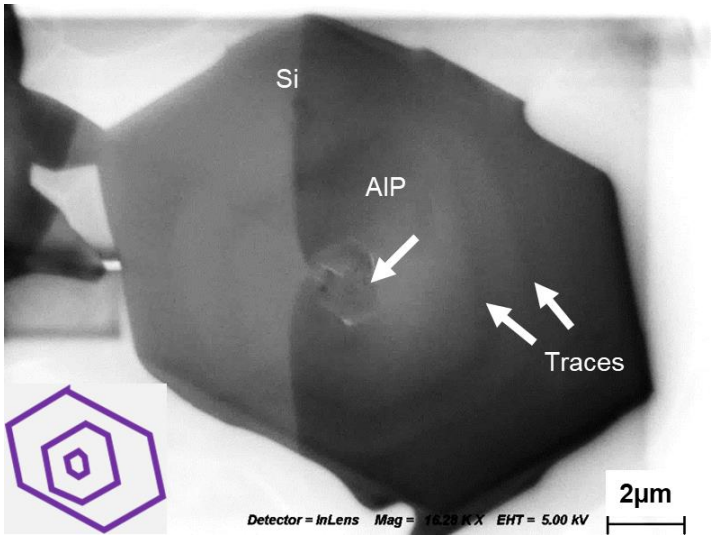

Figure 12. Layer-by-layer growth traces of primary Si crystals on AlP plating crystal. The insert figure showing the sketch of concentric growth traces.

It has been reported that the primary Si crystals exist in the form of dendrites before they join adjacent secondary branches to form faceted crystals which follows layer-by-layer growth mechanism (as known as two-dimensional growth or concentric growth) [11, 39, 40]. The spaces between branches are normally filled by melt and finally become hoppers inside the primary Si. Several researchers have observed the hoppers in Al-18Si or similar alloys [41, 42]. The higher Si concentration (such as 25%) could improve the dendritic growth and therefore result in more obvious hopper structure. As shown in Figure 13 a-c, the hoppers and irregular sub-structures are often observed in faceted primary Si crystals in Al-25Si alloy. However, after phosphorous refinement, the primary Si particles don't have hopper, as shown in Figure 13d. It indicates that the morphologically templated nucleation has an obvious effect on the growth process and final morphology of primary Si crystals. With the help of morphologically templated nucleation triggered by AlP, primary Si phase was forced to skip the initial dendritic growth process and grow layer-by-layer directly, thus maintaining the faceted feature always.

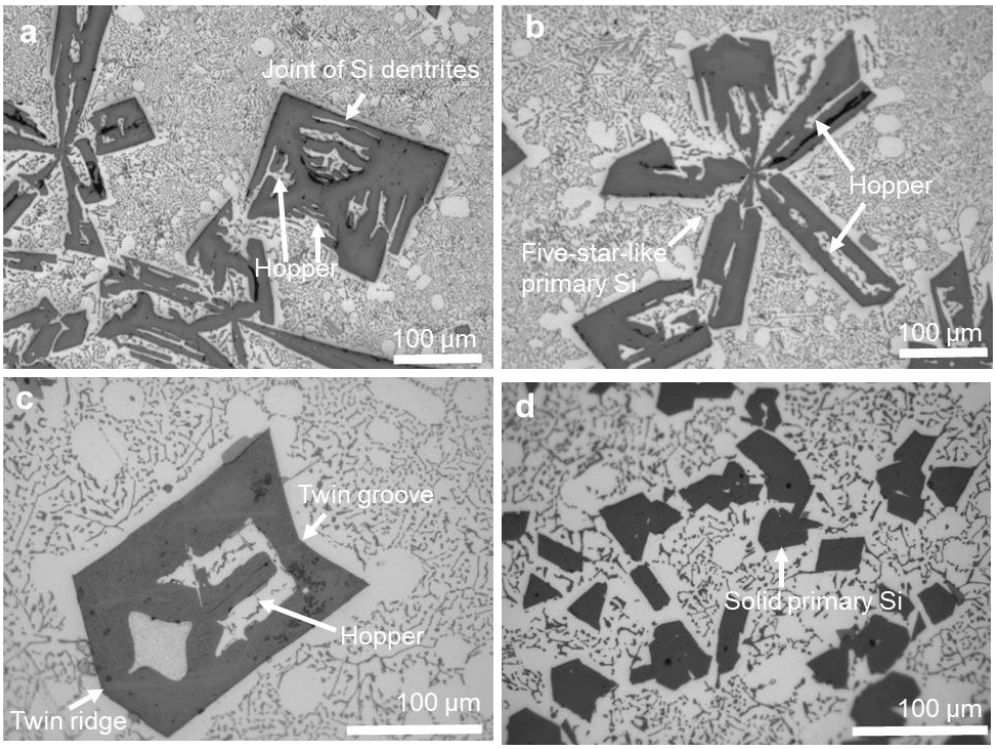

Figure 13. (a-c) Typical hopper-like primary Si crystals in unrefined Al-25Si alloy, and (d) solid primary Si crystals in refined Al-25Si alloy.

5. Conclusions

(1) The existing forms of AlP can be divided into 2 basic categories: non-twin crystals and twin crystals. The former crystals normally have a morphology of truncated octahedron, but also evolve to hexagonal platelets, octahedron, cuboctahedron and cuboid, depending on the ratio of the growth rates along the <100> and <111> directions.

(2) The nucleation of primary Si phase on AlP is a morphologically templated nucleation process. The twin morphological feature of primary Si phase is inherited from AlP twin nuclei by heterogeneous nucleation, while the AlP non-twin nuclei result in the formation of primary Si non-twin crystals. And primary Si crystals are in a cubic-to-cubic orientation relationship with AlP nuclei.

(3) After heterogeneous nucleation, primary Si crystals grow layer-by-layer on AlP

nuclei and remain as faceted crystals. This growth mechanism suppresses the formation of hopper inside primary Si particles and forms primary Si as solid crystals. Meanwhile, the percentage of primary Si twin crystals is increased obviously after phosphorous refinement, although primary Si non-twin crystals are still dominant in the experimental Al-18Si alloys.

Acknowledgements

Financial supports from Innovate UK (grant number 11019) and National Natural Science Foundation of China (grant number 51571133, 51731007 and 52071189) are gratefully acknowledged.

References

[1] S.R. Roland, Google Patents, 1933.
[2] Y. Li, B. Hu, B. Liu, A. Nie, Q. Gu, J. Wang, Q. Li, Acta Materialia, 187 (2020) 51-65.
[3] Z. Fan, Y. Wang, Y. Zhang, T. Qin, X. Zhou, G. Thompson, T. Pennycook, T. Hashimoto, Acta Materialia, 84 (2015) 292-304.
[4] Y. Li, Y. Jiang, B. Liu, Q. Luo, B. Hu, Q. Li, Journal of Materials Science & Technology, 65 (2021) 190-201.
[5] J. Xu, Y. Li, K. Ma, Y. Fu, E. Guo, Z. Chen, Q. Gu, Y. Han, T. Wang, Q. Li, Scripta Materialia, 187 (2020) 142-147.
[6] Y. Li, Y. Jiang, B. Hu, Q. Li, Scripta Materialia, 187 (2020) 262-267.
[7] J. Xu, Y. Li, B. Hu, Y. Jiang, Q. Li, Journal of Materials Science, 54 (2019) 14561-14576.
[8] X. Zhu, W. Jiang, M. Li, H. Qiao, Y. Wu, J. Qin, X. Liu, Metals, 5 (2015) 40-51.
[9] R.Y. Wang, W.H. Lu, L. Hogan, Materials science and technology, 11 (1995) 441-449.
[10] R.Y. Wang, W.-H. Lu, L. Hogan, Metallurgical and Materials transactions A, 28 (1997) 1233-1243.
[11] C. Xu, H. Wang, C. Liu, Q. Jiang, Journal of crystal growth, 291 (2006) 540-547.
[12] H. Singh, A. Gokhale, A. Tewari, S. Zhang, Y. Mao, Scripta Materialia, 61 (2009) 441-444.
[13] J. Wang, Z. Guo, J. Song, W. Hu, J. Li, S. Xiong, Materials & Design, 137 (2018) 176-183.
[14] H. Sonomura, T. Miyauchi, Japanese Journal of Applied Physics, 8 (1969) 1263.
[15] H. Lescuyer, M. Allibert, G. Laslaz, Journal of alloys and compounds, 279 (1998) 237-244.
[16] Q. Zhang, X. Liu, H. Dai, Journal of Alloys and Compounds, 480 (2009) 376-381.
[17] M. Zuo, X. Liu, Q. Sun, K. Jiang, Journal of Materials Processing Technology, 209 (2009) 5504-5508.
[18] Z. Min, L. Xiangfa, Crystal growth & design, 10 (2010) 2443-2446.
[19] J.W. Lee, N.M. Hwang, D.Y. Kim, Journal of Crystal Growth, 250 (2003) 538-545.
[20] M.T. Borgström, K. Mergenthaler, M.E. Messing, U. Håkanson, J. Wallentin, L. Samuelson, M.-E. Pistol, Journal of crystal growth, 324 (2011) 290-295.
[21] F. Wang, Z. Fan, Metallurgical and Materials Transactions A, 50 (2019) 2519-2526.

[22] N. Habibi, A. Samuel, F. Samuel, P. Rochette, D. Paquin, International Journal of Cast Metals Research, 17 (2004) 79-87.
[23] ABB, Prefil-Footprinter Pressure filtration melt cleanliness analyzer: a quick and thorough inclusion control solution. (ABB, 2009) https://search-ext.abb.com/library/Download.aspx?DocumentID=PB%2fPrefilFootprinter-EN&LanguageCode=en&Docu mentPartId=&Action=Launch. Accessed 10 May 2021.
[24] D. Li, M. Zuo, Q. Zhang, X. Liu, Journal of alloys and compounds, 502 (2010) 304-309.
[25] H. Qiao, X. Zhu, T. Gao, Y. Wu, X. Liu, Journal of Materials Science & Technology, 31 (2015) 391-396.
[26] A. Bennett, R. Longini, Physical Review, 116 (1959) 53.
[27] A. Hellawell, Progress in Materials Science, 15 (1970) 3-78.
[28] D. Guan, B. Wynne, J. Gao, Y. Huang, W.M. Rainforth, Acta Materialia, 170 (2019) 1-14.
[29] J. Qin, M. Zuo, T. Gu, X. Liu, Journal of alloys and compounds, 492 (2010) 525-528.
[30] S.-M. Liang, R. Schmid-Fetzer, Acta materialia, 72 (2014) 41-56.
[31] J.D.H. Donnay, D. Harker, American Mineralogist: Journal of Earth and Planetary Materials, 22 (1937) 446-467.
[32] X. Zhu, P. Blake, S. Ji, CrystEngComm, 20 (2018) 3839-3848.
[33] K.W. Benz, W. Neumann, Introduction to crystal growth and characterization, John Wiley & Sons, 2014.
[34] E. Aerts, P. Delavignette, R. Siems, S. Amelinckx, Journal of Applied Physics, 33 (1962) 3078-3080.
[35] X. Liu, Y. Zhang, B. Beausir, F. Liu, C. Esling, F. Yu, X. Zhao, L. Zuo, Acta Materialia, 97 (2015) 338-347.
[36] S.-M. Liang, R. Schmid-Fetzer, Calphad, 42 (2013) 76-85.
[37] T. Nishizawa, Thermodynamics of microstructures, Asm International, 2008.
[38] J. Liu, C.W. Wu, T.T. Tsong, Physical Review B, 43 (1991) 11595.
[39] R.Y. Wang, W.H. Lu, L. Hogan, Journal of Crystal Growth, 207 (1999) 43-54.
[40] I. Sunagawa, Crystals: growth, morphology, & perfection, Cambridge University Press, 2007.
[41] M. Zuo, K. Jiang, X. Liu, Journal of Alloys and Compounds, 503 (2010) L26-L30.
[42] C. Gong, H. Tu, C. Wu, J. Wang, X. Su, Materials, 11 (2018) 456.